

SMA HIGH ANGULAR RESOLUTION IMAGING OF THE LENSED QUASAR APM 08279+5255

M. KRIPS^{1,2}, A.B. PECK¹, K. SAKAMOTO³, G.B. PETITPAS¹, D.J. WILNER², S. MATSUSHITA⁴ AND D. IONO³

Draft version May 29, 2018

ABSTRACT

We present Submillimeter Array observations of the $z=3.91$ gravitationally lensed broad absorption line quasar APM 08279+5255 which spatially resolve the 1.0 mm (200 μm rest-frame) dust continuum emission. At $0''.4$ resolution, the emission is separated into two components, a stronger, extended one to the northeast (46 ± 5 mJy) and a weaker, compact one to the southwest (15 ± 2 mJy). We have carried out simulations of the gravitational lensing effect responsible for the two submm components in order to constrain the intrinsic size of the submm continuum emission. Using an elliptical lens potential, the best fit lensing model yields an intrinsic (projected) diameter of ~ 80 pc, which is not as compact as the optical/near-infrared (NIR) emission and agrees with previous size estimates of the gas and dust emission in APM 08279+5255. Based on our estimate, we favor a scenario in which the 200 μm (rest-frame) emission originates from a warm dust component ($T_d=150\text{-}220$ K) that is mainly heated by the AGN rather than by a starburst (SB). The flux is boosted by a factor of ~ 90 in our model, consistent with recent estimates for APM 08279+5255.

Subject headings: galaxies:high-redshift — galaxies:gravitationally lensed — submillimeter:galaxies — galaxies: individual: (APM 08279+5255)

1. INTRODUCTION

APM 08279+5255 (=APM08) is a strongly lensed broad absorption line (BAL) quasar (Irwin et al. 1998; Lewis et al. 1998) with a very powerful active galactic nucleus (AGN; Soifer et al. 1987). This combination makes it an extremely bright object despite its redshift of $z=3.91$ (Downes et al. 1999). Its bolometric luminosity is thought to be $\sim 5 \times 10^{13} L_\odot$, amplified by up to a factor of 100 by a foreground galaxy which has yet to be identified. Due to the large amplification, broad absorption lines have been detected even in the X-ray (Chartas et al. 2002). Ground-based, *Chandra* and HST observations have suggested that APM08 consists of at least two components separated by $\sim 0''.4$. Ibata et al. (1999, =I99) and Egami et al. (2000, =E00) later detected a third image (their image C), and argued that it is likely a third lensed image of the background QSO instead of the lensing galaxy. Lewis et al. (2002b) obtained optical spectra of the three images using HST/STIS, and showed that the three spectra are quite similar. This indicates that the image C is indeed a third lensed image of APM08. Due to the magnification by the lens, several molecular lines have been detected in APM08 (e.g., Weiß et al. 2007; Guélin et al. 2007; Riechers et al. 2006; Wagg et al. 2006; García-Burillo et al. 2006; Wagg et al. 2005; Lewis et al. 2002a; Downes et al. 1999), suggesting a molecular gas mass of $M_{\text{gas}}(\text{H}_2) = 8 \times 10^{10} m^{-1} M_\odot$ (Riechers et al. 2006, $m \equiv$ magnification factor). The dust mass is estimated to be $M_{\text{dust}} = 5 \times 10^8 m^{-1} M_\odot$ (Downes et al. 1999; Weiß et al. 2007, W07). However,

despite the increasing amount of mm-data, no tight constraints have been set on the size of the dust and/or gas emission which may help to characterize the heating source of the dust and gas, i.e., whether it is in the form of an AGN and/or starburst (SB). Only recently have W07 presented some indirect evidence through brightness temperature arguments that the molecular line and dust emission originate from a compact region with a radius of 100-200 pc. In this *Letter*, we present observations from the Submillimeter Array (SMA) with sufficient resolution ($0''.4$) to resolve the 1.0 mm dust continuum emission in APM08, and lensing models that constrain its intrinsic source size.

2. OBSERVATIONS

We observed the 1.0 mm (200 μm rest-frame) continuum emission in APM08 with the SMA using seven of the eight 6 m antennas in two configurations, with baselines ranging from 20 to 500 meters, in November and December 2006. This results in a synthesized beam of $0''.42 \times 0''.35$ at a position angle (PA) of 141° using robust weighting. The LO frequency was 302.4 GHz (1.0 mm), with each sideband centered 5 GHz to either side. This frequency setup was chosen so that the [N II] line (1461 GHz rest frame) falls within the LSB. However, no significant signal of this line has been found above a 3σ threshold of $9 \text{ Jy beam}^{-1} \text{ km s}^{-1}$, integrated over a velocity range of 1000 km s^{-1} around the expected [N II] frequency. We used Titan as a flux calibrator, 3C111, 3C454.3, J0927+390 and 3C279 as bandpass calibrators, and J0927+390 as a gain calibrator. J0753+538 has been frequently observed throughout the night as a test source to assess the quality of the gain calibration. The phase rms on the gain calibrator is ≤ 40 degrees, resulting in a positional uncertainty of $< 0''.1$ in the test map of J0753+538, which is similar to theoretical noise considerations (Reid et al. 1988), and to a 'seeing' of $< 0.03''$ (\equiv difference between the apparent size of the test quasar and the beam size). The accuracy of the

arXiv:0710.4956v1 [astro-ph] 25 Oct 2007

¹ Harvard-Smithsonian Center for Astrophysics, SMA project, North A'ohoku Place, Hilo, HI, 96720; mkrips@cfa.harvard.edu

² Harvard-Smithsonian Center for Astrophysics, 60 Garden Street, Cambridge, MA 02138

³ National Astronomical Observatory of Japan, Mitaka, Tokyo, 181-8588, Japan

⁴ Academia Sinica Institute of Astronomy and Astrophysics, P.O. Box 23-141, Taipei 106, Taiwan, R.O.C.

flux calibration is around 20%. Weather conditions were good with an atmospheric opacity of $\tau(225 \text{ GHz})=0.06\text{--}0.12$ (recorded at the nearby Caltech Submillimeter Observatory). The data were written into the MIR format originally developed at the Owens Valley Radio Observatory (Scoville et al. 1993), and reduced using SMA-specific MIR tasks in IDL. Following calibration, the data were exported to FITS and imaging and further analysis were done using GILDAS. Both 2 GHz sidebands were merged together in the uv-plane to image the 1.0 mm continuum emission, resulting in an effective rms noise of $1.7 \text{ mJy beam}^{-1}$.

3. RESULTS

The 1.0 mm continuum in APM08 is clearly detected at high angular resolution ($\sim 0''.4$) and high sensitivity ($\text{SNR} \geq 9$; Fig. 1). Using robust weighting, the two lensed images, labeled NE (north-eastern) and SW (south-western) respectively (Fig 1), are clearly separated (by $\sim 0''.4$) from each other. The image positions listed in Table 1 are measured after the image was deconvolved with the synthesized beam. Both absolute positions and the separation are consistent with previous results within the uncertainties (I99, E00). A comparison of the robustly and naturally weighted (angular resolution $\sim 0''.6$) maps indicates similar total fluxes of $\sim 60 \pm 12 \text{ mJy}$ (Table 1). Taking the (single dish) fluxes of 24 mJy at 1.35 mm and of 75 mJy at 0.850 mm and assuming a spectral index of 2.46 (Lewis et al. (1998)), a flux of 50 mJy is expected at 1 mm which is, within the uncertainties, in agreement with the SMA value. This indicates that no flux has been resolved out in our data and the dust emission at $200 \mu\text{m}$ rest-frame cannot be very extended, similar to recent results in APM08 by W07.

The deconvolved size (=FWHM) of the emission in NE appears to be slightly more extended (by $\sim 30\%$) than the synthesized beam (Table 1). An extension in NE is further supported in comparing the peak flux with the spatially integrated flux (Table 1). While they differ by a factor of ~ 2 for NE, they are very similar in SW. This suggests that SW is still unresolved at the high angular resolution of the robustly weighted map. We derive a peak flux ratio of $(\text{NE}/\text{SW})_{\text{peak}} \approx 1.4$ and a spatially integrated flux ratio of $(\text{NE}/\text{SW})_{\text{int}} \approx 3$. The latter is significantly higher than the value found in the (compact) optical/NIR emission of ~ 1.2 (e.g., I99,E00), indicating differential lensing effects. The morphology of the $200 \mu\text{m}$ rest-frame dust emission is in good agreement with that of the CO(1–0) emission of APM08 recently published by Walter et al. (2006). Based on their CO(1–0) map (Fig. 4 in Walter et al. 2006), the NE/SW peak flux ratio is estimated to be ~ 1.5 and the FWHM of NE is estimated to be $0''.3\text{--}0''.4$, which is slightly larger than their beamsize, while SW is clearly unresolved.

4. SIMULATIONS OF THE LENSING EFFECT

Previous lensing models for APM08, obtained by fitting the (compact) NIR emission in E00, fail to reproduce the (extended) emission seen in our submm observations, as in their extended emission models the southern image turns out to be too strong and too extended. Therefore, we have run new simulations⁵ of the gravitational

lensing effect using the code developed by Krips & Neri (Krips et al. 2005, available in GILDAS). We concentrate our simulations on an elliptical lens potential ($\equiv \text{EP}$) similar to previous studies (e.g., E00), although we also tried a single isothermal sphere (SIS) as a lens potential. Although the SIS model fits our submm data, we discarded the SIS models based on the assumption that APM08 is a three-image system and because of the inability of the SIS model to produce an odd number of lensed images.

We varied the parameters of the lensing potential as well as the size of the unlensed source in a reasonable parameter space (see Table 2) until the best agreement between the observed and simulated maps was found, i.e., a model with the lowest reduced χ^2 test (≤ 1). We used the position of the two lensed images (see Table 1), their peak flux ratio ($\text{NE}/\text{SW}=1.4 \pm 0.2$) as well as their (lensed) shape ($\text{FWHM} \simeq 0''.5 \pm 0''.1$ in NE and $\text{FWHM} \leq 0''.2$ in SW) as constraints. We augmented this set of constraints with those from the (compact) optical/NIR emission (e.g., I99, E00; Fig. 1), accounting also for a third lensed image close to NE. This results in 9 observational constraints versus 8 free lensing parameters. We processed the simulated lensed images through a spatial filter defined by the uv-coverage of the observations. This is a more robust approach than simply convolving the simulated data with the synthesized beam of the observations as it also accounts for possible resolution effects (see also Krips et al. 2005). However, based on this set of observational constraints, we could not find any lensing solution that reproduces the optical/NIR and our submm observations. We doubt that this inconsistency is due to mismatched angular resolutions between the optical/NIR and our observations. When starting with an elliptical potential that yields three lensed images and fits the optical/NIR data, NE always turns out to be either too strong or not extended enough compared to SW to match the submm data, or, equivalently, SW is either too extended or not strong enough compared to NE to be consistent with the submm emission. Also, models that fit the submm emission always make the lensed optical/NIR image NE too strong or too extended compared to SW.

A solution to reproduce the optical/NIR and submm data with the same lensing model is to allow different positions between the unlensed optical/NIR and submm sources of emission. This actually increases the number of free lensing parameters to 10. However, we have to handle the observed positions of the lensed images in the optical/NIR and submm case as independent parameters as well, so that the observational constraints also increase to 11. Even though the positional accuracy of the submm and the optical/NIR observations do not yet allow us to substantiate the positional offset ($\sim 0''.08 \pm 0''.07$) between the (lensed) optical/NIR and submm emission and thus also between the unlensed positions, this is still a reasonable approach since it yields a lens model that fits both optical/NIR and submm data. This lens model, called EP(3), is plotted in Fig. 2a and 2b and listed in Table 2. For comparison, Fig. 2c and 2d respectively show simulations in which the unlensed submm source is smaller and larger than the best-fit size. The lens parameters and the position of the unlensed submm source are the same as in Fig 2a and 2b. As the optical/NIR source

⁵ Assumed cosmology: $\Omega_M=0.3$, $\Omega_R=0.0$ and $\Omega_V=0.7$ for a Hubble constant of $H_0=71 \text{ km s}^{-1} \text{ Mpc}^{-1}$ (Spergel et al. 2003), giving

an angular-size distance of $D_A=1.47 \text{ Gpc}$ and $1''=7 \text{ kpc}$.

is very compact in its intrinsic size, the simulation in Fig. 2c is the one to be compared with the optical/NIR observations. The NE/SW ratio for this compact case, however, disagrees with the optical/NIR observations, and the peak separation is clearly wider than what is observed. To correctly reproduce the optical/NIR data, the position of the unlensed source has to be shifted by $\sim 0.003''$ ($\equiv 21$ pc; Fig. 2e). Such an offset between optical/NIR and submm emission could be a consequence of asymmetrically distributed submm emission in APM08. The (best-fit) intrinsic source diameter of the submm emission is $\sim 0.012''$ ($\equiv 84$ pc) and the magnification factor ~ 90 , consistent with recent results from W07.

5. NATURE OF THE DUST EMISSION

W07 and B06 (Beelen et al. 2006) both present a two temperature model for the dust emission in APM08 with an extended 'cold' ($T_d=50-70$ K) and a compact 'warm' ($T_d=160-220$ K) component. The warm dust component is assumed to be heated by the AGN up to a maximum radius of 60-130 pc (W07). W07 also estimate that the dust heating from the AGN can still reach ~ 65 K at a radius of 350 pc and may dominate the cold component as well. However, this estimate has to be considered as an upper limit because of potential self-screening effects in the AGN. Therefore, a significant contribution to the cold component from more extended star formation cannot be completely excluded.

By looking at the dust SED in W07⁶, the contribution of the 'warm' component to the $200\mu\text{m}$ rest-frame emission is $\sim 70\%$. The diameter estimate of 80 pc based on our data lies within the maximum possible diameter of up to 120-260 pc in W07 for the 'warm' dust component. Even when accounting for the apparent offset between AGN and dust emission, this may indicate that the $200\mu\text{m}$ rest-frame emission in APM08 is dominated by the warm dust component although a fractional contribution of the cold component cannot be entirely excluded. Following previous assumptions (e.g., W07) and a similar argumentation as used for Arp 220 (see Downes & Eckart 2007), a SB within a diameter of 80 pc seems unlikely also in APM08 leaving the AGN as the main suspect for the dust heating at $200\mu\text{m}$: similar to Arp 220, APM08 has a very high intrinsic luminosity (for $m=90$) of $\sim 2 \times 10^{12} L_\odot$ at $200\mu\text{m}$ (W07) and, hence, an emission surface brightness of $> 10^{14} L_\odot \text{ kpc}^{-2}$, which is 60 times the luminosity of the nearby SB galaxy M82 in a ~ 4000 times smaller volume (M82's SB disk has a radius of ~ 650 pc; García-Burillo et al. 2000). Although single super-star clusters (SSCs) can reach such a high surface brightness of $\gg 10^{13} L_\odot \text{ kpc}^{-2}$ (e.g. Martín-Hernández, Schaerer, & Sauvage 2005), APM08 would need to harbor > 1000 SSCs that would fill almost its entire central region (typical SSC diameters are ~ 1 pc). This seems to be a rather unlikely scenario. Even if we consider the uncertainties of our models, we can clearly constrain the intrinsic radius to be $\lesssim 150$ pc

⁶ As W07 uses a grey body fit to the dust SED and B06 only a black body, we base our discussion on W07.

(see Fig. 2d), unless the dust 'disk' in APM08 had a very small inclination angle ($i < 30^\circ$), which is, however, not supported by CO observations of W07 who favor $i \approx 70^\circ$. Also in this more conservative case, the inferred surface brightness of APM08 still exceeds that of any SBs seen in the present-day universe by more than an order of magnitude, likely discarding the SB scenario for APM08.

Based on the flux and the deconvolved size determined from the submm-observations, the intrinsic brightness temperature at rest of APM08 can be estimated to be $T_b \approx 30$ K. A comparison to the dust temperature of 220 K of the warm component suggests a dust opacity of $\tau \approx 0.15$ (with $\tau = -\ln(1 - T_b/T_{\text{dust}})$). Assuming the dust temperature of the cold component of 65 K yields a more conservative upper limit of the opacity of ≤ 0.6 at $200\mu\text{m}$ rest-frame, translating to an even smaller upper limit when converted to 1.3 mm. This upper limit is significantly lower than that found for the AGN in Arp 220 of ≥ 0.7 at 1.3 mm by Downes & Eckart (2007); the dust emission in Arp 220 has been suggested to be very similar to that of APM08. This may indicate that the dust emission in APM08 could be either less dense and/or more clumpy than around the AGN of Arp 220. However, given the similar (intrinsic) dust masses of $\sim 10^7 M_\odot$ and the similar intrinsic diameters of ~ 80 pc in both sources, a lower density in APM08 may seem less likely.

6. SUMMARY & CONCLUSION

We have detected the $200\mu\text{m}$ rest-frame continuum emission in APM08 using the SMA with an angular resolution of $\sim 0''.4$. The two (main) lensed images are clearly separated with a combined flux of $\sim 60 \pm 12$ mJy. Simulations of the gravitational lensing effect in this system yield a diameter of the intrinsic (submm) continuum emitting region of ~ 80 pc and magnification factor of 90. Our data and simulations seem to be only consistent with a lensing scenario including a third lensed image of APM08 close to NE if the position of the compact optical/NIR emission and the position of the extended submm emission are offset from each other before lensing by $\sim 0''.003$ ($\equiv 21$ pc). Further (sub)mm observations may be beneficial to determine whether such a positional offset is indeed necessary or more complicated lens potentials have to be considered. Given our size estimate, we favor a scenario in which the $200\mu\text{m}$ emission originates from a warm dust component that is supposed to be mainly heated by the AGN rather than by a SB.

The SMA is a joint project between the Smithsonian Astrophysical Observatory and the Academia Sinica Institute of Astronomy and Astrophysics and is funded by SAO and ASIAA. We thank Drs Downes and Neri for fruitful discussions and the referee for a thorough review of the paper. We are grateful to the dedicated SMA staff who make these observations possible.

REFERENCES

- Downes, D., & Eckart, A., 2007, *A&A*, 468, L57
- Downes, D., Neri, R., Wiklind, T., Wilner, D. J., Shaver, P. A 1999, *ApJ*, 513, L1
- Egami, E., et al., 2000, *ApJ*, 535, 561
- Martín-Hernández, N.L., Schaerer, D., Sauvage, M., 2005, *A&A*, 429, 449
- García-Burillo, S.; Martín-Pintado, J.; Fuente, A.; Usero, A.; Neri, R., 2002, *ApJ*, 575, L55
- García-Burillo, S., et al., 2006, *ApJ*, 645, L17
- Guélin, M., et al., 2007, *A&A*, 462, L45
- Ibata, R. A., Lewis, G. F., Irwin, M. J., Lehár, J. & Totten, E. J. 1999, *AJ*, 118, 1922
- Irwin, M. J., Ibata, R. A., Lewis, G. F., Totten, E. J. 1998, *ApJ*, 505, 529
- Krips, M., Neri, R., Eckart, A., Downes, D., Martín-Pintado, J., Planesas, P., 2005, *A&A*, 431, 879
- Lewis, G. F.; Chapman, S. C.; Ibata, R. A.; Irwin, M. J.; Totten, E. J., 1998, *ApJ*, 505, L1
- Lewis, G. F.; Carilli, C.; Papadopoulos, P.; Ivison, R. J., 2002, *MNRAS*, 330, L15
- Lewis, G. F., Ibata, R. A., Ellison, S. L., Aracil, B., Petitjean, P., Pettini, M., 2002, *MNRAS*, 334, L7
- Reid, M. J., et al., 1988, *ApJ*, 330, 809
- Riechers, D. A., et al., 2006, *ApJ*, 650, 604
- Scoville, N. Z., et al., 1993, *PASP*, 105, 1482
- Soifer, B. T., et al., 1987, *ApJ*, 320, 238
- Spergel, D. N., et al., 2003, *ApJS*, 148, 175
- Wagg, J.; Wilner, D. J.; Neri, R.; Downes, D.; Wiklind, T., 2005, *ApJ*, 634, L13
- Wagg, J.; Wilner, D. J.; Neri, R.; Downes, D.; Wiklind, T., 2006, *ApJ*, 651, 46
- Walter, F.; Riechers, D. A.; Carilli, C. L.; Bertoldi, F.; Weiss, A.; Cox, P., 2007, "From Z-Machines to ALMA", eds. A.J. Baker, J. Glenn, A.I. Harris, J.G. Mangum, M.S. Yun, ASP Conf. Series, Vol. 375, p. 182
- Weiß, A., et al., 2007 (W07), *A&A*, 467, 955

TABLE 1
OBSERVATIONAL PARAMETERS OF APM 08279+5255

Component	$\Delta\alpha^a$ ($''$)	$\Delta\delta^a$ ($''$)	$S_{1\text{mm}}^{\text{peak } b}$ (mJy beam $^{-1}$)	$S_{1\text{mm}}^{\text{int } c}$ (mJy)	Deconvolved Size maj. \times min., P.A. ($'' \times ''$, $^\circ$)
Total ^d	-0.10 ± 0.03	-0.10 ± 0.03	34 ± 2	60 ± 12	$(0.8 \times 0.7) \pm 0.1, (52 \pm 5)$
NE ^e	0.00 ± 0.04	0.00 ± 0.04	21 ± 2	46 ± 5	$(0.5 \times 0.2) \pm 0.1, (50 \pm 20)$
SW ^e	-0.28 ± 0.06	-0.26 ± 0.06	15 ± 2	15 ± 2	≤ 0.2

^a The offsets are with respect to $\alpha_{\text{J2000}}=08\text{h}31\text{m}41.69\text{s}$ and $\delta_{\text{J2000}}=52\text{d}45\text{m}17.5\text{s}$. The positional errors comprise the statistical errors from the Gaussian fit to the data in the uv-plane and uncertainties from the calibration.

^b Peak flux. Errors are based on the statistical noise in the map.

^c Spatially integrated flux. The flux errors include the statistical uncertainties from the fit and in the case of the total flux also the calibrational uncertainties, which are estimated to be $\sim 20\%$.

^d Based on the naturally weighted map and an elliptical gaussian fit.

^e Based on the robustly weighted map and an elliptical (circular) gaussian fit for NE (SW).

TABLE 2
PARAMETERS OF THE BEST-FIT GRAVITATIONAL LENS MODEL.

	θ_{E}^b ($''$)	ϵ^c	PA ^d ($^\circ$)	θ_c^e ($''$)	$(\Delta\alpha, \Delta\delta)^f$ ($''$, $''$)	θ_s^g ($''$)	m^h
EP(3) ^a	0.31	0.008	-30	0.21	$(-0.218, -0.158)$	0.012	90

^a Elliptical potential with three lensed images; we allowed the unlensed source position to be variable between the optical/NIR and our submm data (see text).

^b Einstein radius θ_{E} ; tested parameter range: $\theta_{\text{E}}=0''.1-0''.4$

^c Ellipticity ϵ ; tested parameter range: $\epsilon=0-0.2$

^d Positional angle PA (from N to E): tested range -90 to $+90^\circ$

^e Core radius θ_c ; tested parameter range: $\theta_c=0-0.3''$

^f The position of the unlensed source is with respect to the lensed component NE. The lens position is at $(\Delta\alpha, \Delta\delta)=(-0''.210, -0''.150)$.

^g θ_s =intrinsic source diameter; tested range: $0''.001-0''.3$ ($\equiv 0.007-2.1$ kpc)

^h m =magnification factor

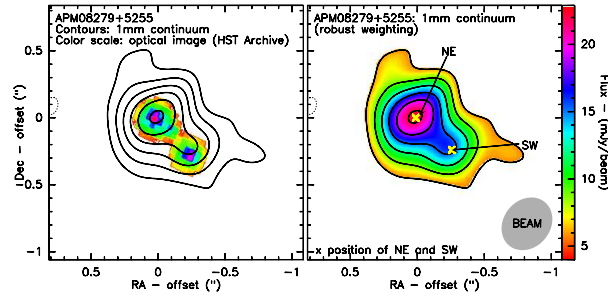


FIG. 1.— *Left*: HST image of APM08 observed with the WFCP2/F814W filter (STScI archive). The black contours represent the 1mm continuum emission. *Right*: Continuum image at the observed wavelength of 1.0 mm of APM08 with robust weighting. Contours start at $\pm 3\sigma$ in steps of 2σ ; 1σ corresponds to $1.7 \text{ mJy beam}^{-1}$. The yellow crosses mark the (deconvolved) position of the two lensed images; they are thus slightly more separated than the peaks of the contour image. The image is referenced to component NE (Table 1).

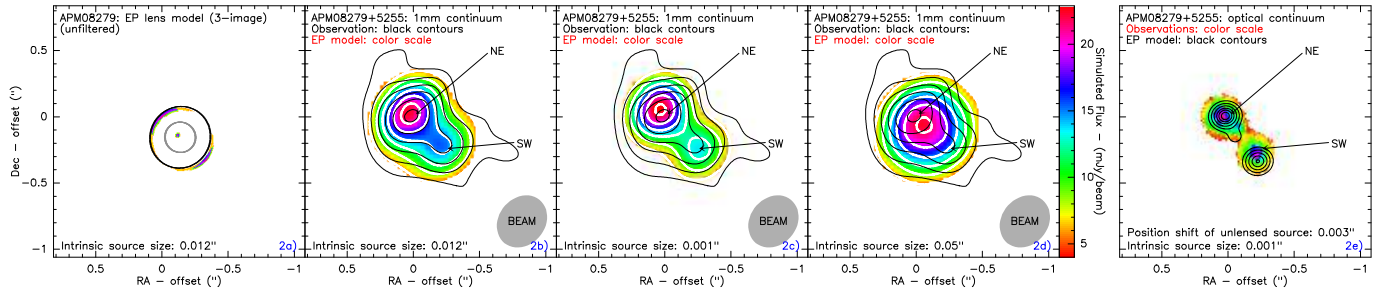


FIG. 2.— Simulations (*color scale and white contours*) based on an elliptical lens model with three lensed images: EP(3). The simulated emission is overlaid with the observed emission (*black contours*). Contours are the same as in Fig. 1. The model with the best-fit source size for the submm data are shown in *2a*) (unfiltered) and in *2b*) (spatially filtered). *2c*) and *2d*) columns show the best-fit model with the smallest and largest unlensed source sizes, while *2e*) shows the model for the optical/NIR case (smoothed to $0''.15$). The models in *2c*) and *2d*) refers to the (unlensed) submm position; the (unlensed) optical/NIR position is offset by $\sim 0''.003$ in *2e*) from the (unlensed) submm position (see Section 4).